Electronic structures of Mn-induced phases on GaN(0001)

Y. Qi, G. F. Sun, M. Weinert, and L. Li*
Department of Physics and Laboratory for Surface Studies, University of Wisconsin, Milwaukee, Wisconsin 53211, USA
(Received 18 June 2009; revised manuscript received 6 November 2009; published 17 December 2009)

We investigate the atomic and electronic structures of Mn-incorporated GaN(0001) surface by scanning tunneling microscopy and first-principles calculations. The incorporation of Mn at room temperature initially leads to a disordered phase, and subsequently an ordered (3×3) reconstruction at ~0.5 ML Mn coverage. The (3×3) exhibits a honeycomb structure for sample bias below −0.5 V, and appears as a closed-packed structure above −1.2 V, which is attributed to antiferromagnetic ordering induced by Mn atoms. Incorporation of the same amount of Mn at an elevated substrate temperature of 300 °C produces an additional phase with local (5×5) periodicity, consisting of two types of trimers: one with three spots of equal intensity and the other with uneven intensities. This disparity in intensity can be resolved using a Fe-coated W tip, which is attributed to enhanced spin-dependent tunneling between the Mn-induced minority states and the Fe-induced states of the functionalized W tip.

DOI: 10.1103/PhysRevB.80.235323 PACS number(s): 68.35.bg, 68.37.Ef, 73.20.At, 75.70.Rf

I. INTRODUCTION

Diluted magnetic semiconductors (DMSs) have shown great potential for the next-generation spintronic devices which manipulate both the spin and charge of electrons to process information.[1,2] Mn-doped GaN has garnered special attention because its Curie temperature (T_C) is predicted to be higher than room temperature.[3] However, extensive theoretical and experimental investigations have yielded considerable conflicting observations: ferromagnetic (FM) ordering with T_C varying from 10 to 954 K, antiferromagnetic (AFM) ordering, as well as spin glass behavior, have all been reported.[4–18]

These inconsistencies may stem from the different growth conditions used, which can lead to the formation of a variety of defects,[18] as well as the presence of Mn clusters and secondary phases. For example, Mn_xN_y phases that may have formed during growth have been suggested as being, at least partially, responsible for the ferromagnetic behavior of (Ga,Mn)N.[17] In addition, calculations have indicated that while FM ordering is expected in the bulk, AFM coupling can exist on or near the surface layers, due to the greater contraction of Mn-Mn and Mn-N bond length on GaN $(11\bar{2}0)$ surfaces.[19,20] Furthermore, the incorporation of Mn on the GaN(0001) (2×2) surface has been found to be concentration and temperature dependent: at low concentrations, Mn atoms prefer random substitution. At higher Mn concentrations, growth temperature also plays a role: Mn atoms tend to form ferromagnetic planar pairs or larger clusters in the (0001) plane at low temperatures, and zigzag ferromagnetic columns at higher temperatures.[21] Clearly, a better understanding of the incorporation of Mn on GaN surface at the atomic scale, particularly on a substrate orientation and surface that is molecular beam epitaxy (MBE) growth relevant, is crucial for improving the growth processes and ultimately to synthesize homogeneous GaN-based DMS for practical applications.

In this work, we investigate the atomic and electronic structures of Mn-incorporated GaN(0001) pseudo-1×1 (denoted "1×1" hereafter) surface by scanning tunneling microscopy (STM) and first-principles calculations. Depending on Mn coverage and incorporation temperature, one disordered and two ordered phases, (3×3) and (5×5), are observed. The atomic structure of both ordered structures is studied using a nominal W tip as well as an Fe-coated tip.[22] Based on the calculated energetics of various Mn-incorporation configurations, we propose a mechanism for Mn incorporation, as well as structural models for these phases.

II. EXPERIMENT

The GaN films were grown by plasma-assisted MBE on 6H-SiC(0001) substrates at 600 °C. The film surface exhibits a metallic "1×1" structure which is typically seen for GaN films grown under Ga-rich conditions, consisting of ~2 ML Ga on top of the Ga-terminated GaN.[23–25] Mn was deposited on this surface at a rate of 0.1 ML/min at room temperature as well as at an elevated temperature of 300 °C. STM imaging was carried out in constant current mode with an Omicron variable temperature STM interconnected to the MBE chamber. W tips were prepared by electrochemical etching, some of which were then subsequently coated with more than 10 ML of Fe in ultrahigh vacuum. Characterization by scanning electron microscopy and energy dispersive spectroscopy indicate that the radius of the Fe-coated W tip is ~300 nm.[26] Unless otherwise specified, the images shown are taken with a W tip.

III. RESULTS

STM images of the GaN surface after Mn incorporation at room temperature and 300 °C are shown in Fig. 1. At low Mn coverage, part of the GaN "1×1" region is converted into a disordered structure [Fig. 1(a)]. With increasing Mn coverage, the population of this phase grows to cover most of the surface [Fig. 1(b)], while a new ordered structure with a (3×3) periodicity begins to nucleate within it. At about 0.5 ML Mn, the (3×3) phase populates the majority of the surface, as shown in Fig. 1(c). When the same amount of Mn

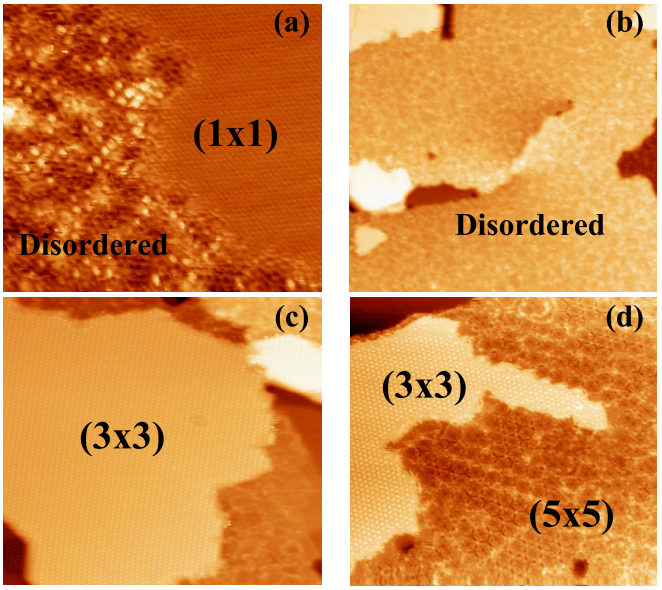

FIG. 1. (Color online) STM images of structures observed after Mn incorporation on the GaN(0001)-"1×1" at room temperature. (a) At the beginning of Mn incorporation, the surface is converted to a disordered phase (sample bias: −0.5 V, tunneling current: 0.3 nA, and image size: 20×20 nm^2). (b) With increasing Mn coverage, the disordered phase covers the majority of the surface (sample bias: −1.3 V, tunneling current: 1.0 nA, and image size: 94×94 nm^2). (c) At 0.5 ML Mn, an ordered (3×3) phase is formed (sample bias: −1.4 V, tunneling current: 1.0 nA, and image size: 50×50 nm^2). (d) Reconstruction upon Mn deposition at 300 °C. Both (3×3) and (5×5) are observed (sample bias: −0.15 V, tunneling current: 2.0 nA, and image size: 50×50 nm^2).

(0.5 ML) is deposited at 300 °C, a new phase with partial ordering is observed in addition to the (3×3) reconstruction [Fig. 1(d)]. Since the two phases are always found to coexist, the critical Mn coverage for the formation of each phase is not well defined.

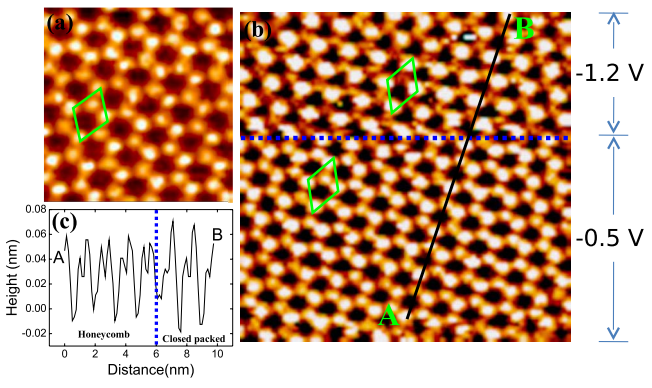

FIG. 2. (Color online) (a) Atomic resolution STM image of the (3×3) structure (sample bias: −0.3 V, tunneling current: 1.0 nA, and image size: 5×5 nm^2); (b) The topography changes from honeycomb to closed-packed structure as the bias voltage is switched from −0.5 to −1.2 V; dotted line marks the position of the change (tunneling current: 1.0 nA and image size: 9.5×9.5 nm^2). The parallelograms mark the unit cells in both cases. (c) Profile of line AB marked in Fig. 2(b) showing the height difference between neighboring protrusions for the honeycomb and closed-packed structure.

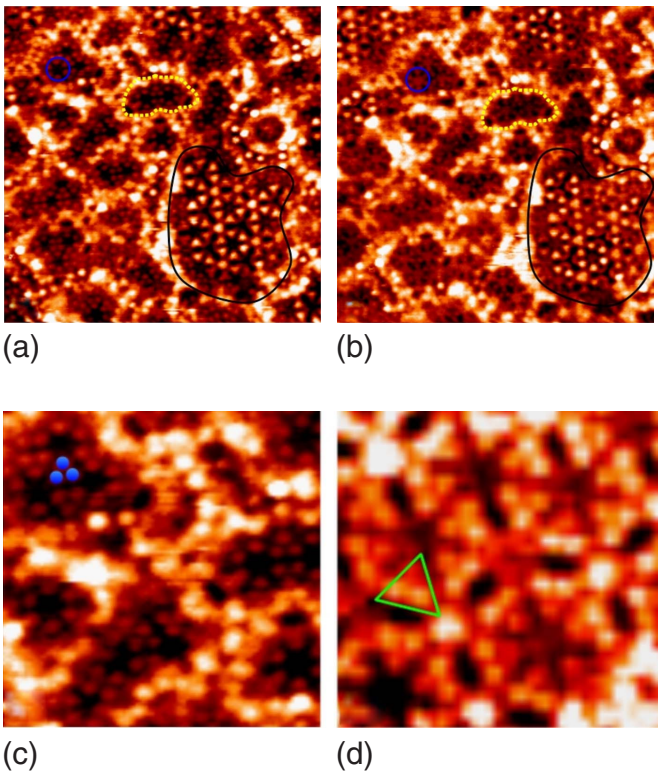

FIG. 3. (Color online) (a) STM image of the local (5×5) obtained with sample bias at −0.7 V, tunneling current at 3.0 nA (image size: 22×22 nm^2). Variant I and II are marked by dashed and solid outlines, respectively. (b) STM image of the same location as in (a) but with sample bias at 0.7 V, tunneling current at 3.0 nA. (c) Closed-up view of the triangular features of variant I. (d) STM image of variant II taken using a Fe/W tip. [Sample bias: −0.4 V, tunneling current: 0.5 nA, and image size: 9×9 nm^2 for (c) and 5×5 nm^2 for (d)].

The (3×3) structure exhibits a strong bias dependence. For sample bias below −0.5 V, a honeycomb structure is observed [Fig. 2(a)], though the contrast of the corner spots alternates slightly between bright and dim. When the sample bias is changed from −0.5 V (bottom half) to −1.2 V (top half), this contrast becomes much more enhanced, as shown in Fig. 2(b). As a result, the honeycomb now appears as a closed-packed structure. The difference in height between the bright and dim spots can be clearly seen in the line profile across AB, as shown in Fig. 2(c). For the honeycomb, the height difference from peak to valley is 0.7 Å, and between the neighboring protrusions is 0.1 Å. The closed-packed unit cells exhibit a qualitatively similar profile, however, with an enhanced height difference of 0.9 Å from peak to valley, and 0.3 Å between the neighboring bright and dim protrusions, three times that of the honeycomb structure.

The high-temperature phase typically appears in small patches separated by bright domain boundaries (one of which is outlined by the dashed line), as shown in Fig. 3. The lattice spacing between the corner holes (as marked by a circle) is 16 Å, giving rise to a local (5×5) periodicity. At first glance this structure is qualitatively similar to that of the Si(111) (5×5).[27] However, unlike the silicon surface, the corner holes appear differently depending on bias polarities:

while it appears as a depression ("hole") in filled state images [Fig. 3(a)], it appears as a protrusion in empty-state images [Fig. 3(b)].

Close examination of the structure reveals that there are two variants of the (5×5): the majority (variant I) consists of trimers with three well-resolved bright spots with equal intensity [one of which is marked by a triad of three circles in Fig. 3(c)]; the rest (variant II), as those enclosed by the solid line in Fig. 3(a), exhibit only triangular shapes. Interestingly, the details of these triangular features can be resolved clearly using a Fe-coated W tip, as shown in Fig. 3(d) (marked by a triangle). They are, in fact, also trimers consisting of three spots with uneven intensities—the two "outer" spots are brighter than the "inner" spot—which gives rise to additional ordering: a pair of bright spots facing each other.

IV. DISCUSSIONS

To elucidate the energetics of various Mn-incorporation configurations and the nature of their bonding, first-principles calculations using the full-potential linearized augmented plane-wave method,[28,29] as implemented in *flair*,[30] have been carried out. We model the Ga-rich GaN(0001) surface using nine GaN bilayers with an additional two layers of Ga in a $\sqrt{3}\times\sqrt{3}$ structure; these additional layers of Ga were either in the "1×1" structure (with four Ga atoms in the top layer) or in a tetrahedral Ga bilayer. The in-plane GaN lattice constant is fixed at the calculated value of $a=3.18$ Å $(c/a=1.626)$. To check the Mn-Mn distance dependence and relative magnetic alignment, additional calculations were done using 3×3 and $\sqrt{3}R30°\times3$ (with six atoms per layer) structures with four GaN bilayers as the substrate (plus two Ga layers). For the nine (four) GaN-bilayer substrate calculations, the bottom three (two) layers of the film were kept fixed at the calculated bulk positions, but the positions of the other atoms were allowed to relax. The calculations were done in a film, rather than a supercell, geometry in order to avoid artificial interactions between the slabs. The Brillouin zone was sampled using an $8\times8\times2$ mesh for the $\sqrt{3}\times\sqrt{3}$ calculations, and equivalent sets for the other calculations. The energetics reported here require the differences between sets of calculations (e.g., the various clean surfaces, adatoms, and substitution configurations), so tests were done to ensure that the results were converged with respect to basis size, k-point sampling, etc. The calculations using the different surface cells gave consistent results for systems that could be treated using all of the cells. To address the incorporation of Mn at different sites, possibilities ranging from the top GaN bilayer to adatom sites were considered, both for the "1×1" and for the Ga-bilayer structures.

The results suggest that the transformation from the "1×1" to the (3×3) structure proceeds by first incorporating Mn in the upper layer of the "1×1". The "1×1" structure is nominally more stable than the Ga-bilayer structure (by 0.07 eV), but the incorporation of Mn [cf. Fig. 4(a)] reverses the relative stabilities of these two phases. Specifically, the configuration with Mn in a substitutional site in the top layer and Ga adatoms at T_4 sites (to account for the extra Ga of the "1×1") is energetically more favorable, by 0.55 eV/incorporated Mn, than a "1×1" structure that simply incorporates Mn. Therefore, the incorporation of Mn would favor the formation of a Ga-bilayer structure. In addition, there is also a strong preference for the Ga adatom to be next to the substitutional Mn (by 0.41 eV), rather than having the Ga adatom neighboring another Ga, in contrast to the cases of Ge and Si incorporation on the same surface.[31,32]

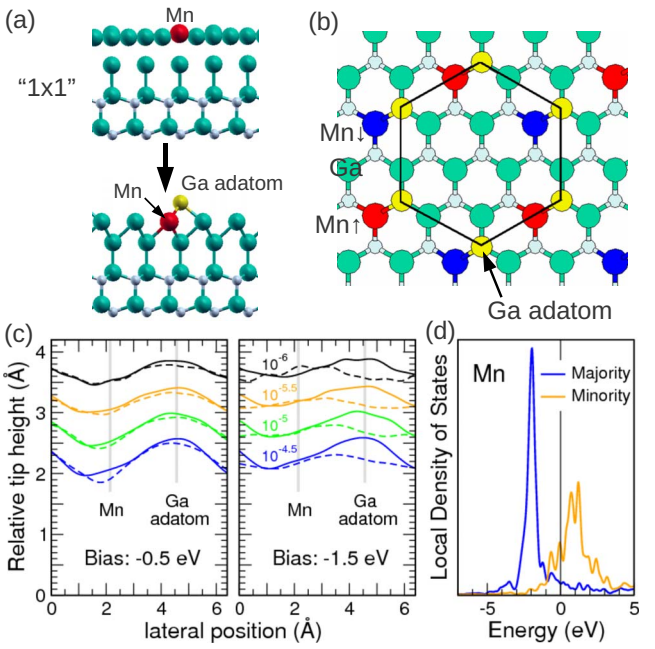

FIG. 4. (Color online) (a) The addition of Mn to the "1×1" structure causes a structural change into a tetrahedral Ga bilayer with a Ga adatom. (b) The resulting (3×3) structure consists of AFM-coupled Mn atoms and Ga adatoms. (c) Calculated line profiles (solid lines: local majority spin and dashed lines: minority spin) along a line through Mn and its neighboring Ga adatoms for two biases for various constant values of the energy-integrated (position-dependent) density of states. (d) Calculated spin-resolved local density of states for Mn.

More importantly, with additional Mn incorporation into the newly formed bilayer structure, there is also a preference (~0.05 eV/Mn) for the Mn atoms to be second nearest neighbors in the same plane, suggesting that the formation of a new reconstruction is favored rather than Mn clustering. (The preference for Mn to be surrounded by Ga is consistent with the bulk phase diagram and the tendency in compounds to have unlike neighbors.) Not surprisingly, the Mn atoms also prefer to couple antiferromagnetically (~0.10 eV/Mn). The smallest reconstruction that can satisfy these two conditions, i.e., second-nearest-neighbor arrangements for Mn atoms and antiferromagnetic coupling between them, is a honeycomb structure with a (3×3) periodicity, as shown in Fig. 4(b). Note that this arrangement also averts the magnetic frustration that would have occurred if there were an additional Mn at the center of the honeycomb, i.e., a $(\sqrt{3}\times\sqrt{3})$ structure.

The calculated (energy-integrated) position-dependent densities of states (DOS), $\int d\varepsilon n(\boldsymbol{r},\varepsilon)$, provide direct insights

into the bias-dependent behavior shown in Fig. 2(b). A simple model of STM relates the relative height of the tip to contours of constant DOS; the bias dependence is reflected by the range of energies of the states that are included in the density. In Fig. 4(c), the contours of constant density for biases $E=-0.5$ and -1.5 eV (which includes the occupied states between the Fermi level and E) are plotted for the local majority (solid lines) and minority (dotted lines) states along a profile through a Mn atom and its neighboring Ga adatom. The Ga adatom is clearly the most prominent feature, however, a distinct difference in height for the Mn atoms is also observed depending on their magnetic orientation. The height difference is calculated to be ~ 0.1 Å for a bias of -0.5 eV and increases to about 0.3–0.4 Å for -1.5 eV. This difference—which is independent of the choice of contour—is simply related to the Mn local DOS (LDOS), as shown in Fig. 4(d): the large peak in the majority LDOS is not sampled for the smaller bias. These findings are in excellent agreement with the experimental results presented in Fig. 2.

These calculations also shed light on the nature of the (5×5). As discussed above, the substitutional incorporation of Mn causes the replaced Ga atom to form an adatom near the Mn. Since the calculations show that the most prominent LDOS on the surface originates from Ga atoms [Fig. 4(c)], it suggests that the trimer spots of the (5×5) are Ga adatoms. The difference between the two variants (with even and uneven trimers) is likely due to whether there is a Mn atom incorporated within the layer below, since the contrast arises from the spin-dependent tunneling between the Fe/W tip and the Ga adatom bonded to a Mn atom from the layer below. Our calculations of the Fe/W tip indicate that there is an occupied state around 0.5 eV below the Fermi level (E_F),[33] which would enhance tunneling into the Mn-induced minority states at ~ 1 eV above E_F. The fact that this contrast between the trimer spots can be resolved using an Fe-coated W tip is consistent with it being related to the Ga adatoms bonded to Mn atoms underneath.

The observation that this phase is only formed at elevated temperatures may be due to the enhanced Mn migration at higher temperatures, which leads to the formation of Mn-rich domains, while the excess Ga atoms (displaced by Mn incorporation and from the formation of the Ga-bilayer structure) form bright boundaries. In addition, since Mn prefers Ga to be nearest in-plane neighbors, it also explains the secondary ordering observed in these trimers, where the dimmer spots are always the inner spots. Nevertheless, to confirm the precise placements of the substitutional Mn atoms underneath the Ga bilayer, more extensive theoretical calculations are necessary.

In conclusion, using STM and first-principles calculations, we have investigated the structural and electronic properties of Mn-incorporated GaN(0001). A disordered phase and a (3×3) structure are found at room temperature, while coexistence of (5×5) and (3×3) are observed at elevated temperatures. The ordered (3×3) phase exhibits a honeycomb/closed-packed structure depending on the bias voltage, and a structural model is proposed where the Mn atoms are in an antiferromagnetic arrangement. The (5×5) consists of two types of triangular features, one of which can be resolved by a Fe/W tip and is attributed to enhanced spin-dependent tunneling between the Mn-induced minority states and states of the Fe-coated W tip.

ACKNOWLEDGMENTS

Financial support for this work is provided by the Department of Energy (Grant No. DE-FG02-07ER46228) and NSF (Grant No. DMR-0706359).

*lianli@uwm.edu

[1] H. Ohno, Science **281**, 951 (1998).
[2] S. J. Pearton, D. P. Norton, R. Frazier, S. Y. Han, C. R. Abernathy, and J. M. Zavada, IEEE Proc. Circuits Dev. Sys. **152**, 312 (2005).
[3] T. Dietl, H. Ohno, F. Matsukura, J. Cibert, and D. Ferrand, Science **287**, 1019 (2000).
[4] M. E. Overberg, C. R. Abernathy, S. J. Pearton, N. A. Theodoropoulou, K. T. McCarthy, and A. F. Hebard, Appl. Phys. Lett. **79**, 1312 (2001).
[5] M. L. Reed, N. A. El-masry, H. H. Stadelmaier, M. K. Ritums, M. J. Reed, C. A. Parker, J. C. Roberts, and S. M. Bedair, Appl. Phys. Lett. **79**, 3473 (2001).
[6] G. T. Thaler, M. E. Overberg, B. Gila, R. Frazier, C. R. Abernathy, S. J. Pearton, J. S. Lee, S. Y. Lee, Y. D. Park, Z. G. Khim, J. Kim, and F. Ren, Appl. Phys. Lett. **80**, 3964 (2002).
[7] T. Sasaki, Saki Sonoda, and Yoshiyuki Yamamoto, J. Appl. Phys. **91**, 7911 (2002).
[8] S. Sonoda, S. Shimizu, T. Sasaki, Y. Yamamoto, and H. Hori, J. Cryst. Growth **237-239**, 1358 (2002).
[9] S. S. A. Seo, M. W. Kim, Y. S. Lee, T. W. Noh, Y. D. Park, G. T. Thaler, M. E. Overberg, C. R. Abernathy, and S. J. Pearton, Appl. Phys. Lett. **82**, 4749 (2003).
[10] Y. Shon, Young Hae Kwon, Sh. U. Yuldashev, Y. S. Park, D. J. Fu, D. Y. Kim, and T. W. Kand, J. Appl. Phys. **93**, 1546 (2003).
[11] H. Choi, H. Seong, J. Chang, K. Lee, Y.-J. Park, J. Kim, S. Lee, R. He, T. Kuykendall, and P. Yang, Adv. Mater. (Weinheim, Ger.) **17**, 1351 (2005).
[12] M. Zając J. Gosk, M. Kamińska, A. Twardowski, T. Szyszko, and S. Podsiadło, Appl. Phys. Lett. **79**, 2432 (2001).
[13] S. Dhar, O. Brandt, A. Trampert, L. Daweritz, K. J. Friedland, K. H. Ploog, J. Keller, B. Beschoten, and G. Guntherodt, Appl. Phys. Lett. **82**, 2077 (2003).
[14] K. H. Ploog, S. Dhar, and A. Trampert, J. Vac. Sci. Technol. B **21**, 1756 (2003).
[15] K. Ando, Appl. Phys. Lett. **82**, 100 (2003).
[16] Tobias Graf, Sebastian T. B. Goennenwein, and Martin S. Brandt, Phys. Status Solidi B **239**, 277 (2003).
[17] M. Zając, J. Gosk, E. Grzanka, M. Kamińska, A. Twardowski, B. Strojek, T. Szyszko, and S. Podsiadło, J. Appl. Phys. **93**, 4715 (2003).
[18] D. J. Keavney, S. H. Cheung, S. T. King, M. Weinert, and L. Li,

Phys. Rev. Lett. **95**, 257201 (2005).
[19] Q. Wang, Q. Sun, and P. Jena, Phys. Rev. Lett. **95**, 167202 (2005).
[20] Q. Wang, Q. Sun, and P. Jena, Phys. Rev. Lett. **93**, 155501 (2004).
[21] Shiqiang Hao and Zhenyu Zhang, Phys. Rev. Lett. **99**, 166101 (2007).
[22] O. Pietzsch, A. Kubetzka, M. Bode, and R. Wiesendanger, Science **292**, 2053 (2001).
[23] J. E. Northrup, J. Neugebauer, R. M. Feenstra, and A. R. Smith, Phys. Rev. B **61**, 9932 (2000).
[24] M. Harland and L. Li, Appl. Phys. Lett. **89**, 132104 (2006).
[25] S. T. King, M. Weinert, and L. Li, Phys. Rev. Lett. **98**, 206106 (2007).
[26] M. Bode, Rep. Prog. Phys. **66**, 523 (2003).
[27] Y. Wei, L. Li, and I. S. T. Tsong, J. Vac. Sci. Technol. A **13**, 1609 (1995).
[28] E. Wimmer, H. Krakauer, M. Weinert, and A. J. Freeman, Phys. Rev. B **24**, 864 (1981).
[29] M. Weinert, G. Schneider, R. Podlouck, and J. Redinger, J. Phys.: Condens. Matter **21**, 084201 (2009).
[30] http://www.uwm.edu/~weinert/flair.html
[31] Y. Qi, S. T. King, S. H. Cheung, M. Weinert, and L. Li, Appl. Phys. Lett. **92**, 111918 (2008).
[32] A. L. Rosa and J. Neugebauer, Phys. Rev. B **73**, 205314 (2006).
[33] The Fe/W tip is modeled by an Fe pyramid on a three-layer $c(4\times4)$ W (110). The calculations indicate that the apex Fe atom gives a large enhancement of the magnetic moment ($2.78\mu_B$/atom) compared to that of bulk Fe and to the Fe atoms directly in contact with W slab ($2.1-2.3\mu_B$/atom). The enhancement of the magnetic moment of the topmost Fe atom is reminiscent of increased moments at surfaces and is due to a shift of the peaks in the DOS related to band narrowing. The minority spin channel has an especially sharp peak at 0.5 eV below E_F. Tunneling of electrons between Mn-induced states and these localized states allows the imaging of the energy- and position-dependent density of states not accessible by a W tip. In addition, the spatially resolved DOS indicate these states have *d* character pointing out of the surface, which would further enhance the resolution.